

# Electrostatic Accelerated Electrons Within Information Horizons Exert Bidirectional Propellant-Less Thrust

Becker, F. M.      Bhatt, Ankur S.

December 16, 2021

## Abstract

During internal discharge (electrical breakdown or field emission transmission), thin symmetric capacitors accelerate slightly towards the anode; an anomaly that does not appear obvious using standard physics. The effect can be predicted by core concepts of a model called quantised inertia (MiHsC) which assumes inertia of accelerated particles, such as electrons, is caused by Unruh radiation. This discrete Unruh radiation forms standing waves between the particle's boundaries from the Rindler horizon to the confinement horizon. These waves are established based on special relativity in concert with quantum mechanics. Electrons accelerate toward the anode and are assumed to encounter an inhomogeneous Unruh radiation condition causing a force to modify their inertial mass. To conserve momentum, the overall mechanical system moves in the direction of the anode. This resulting force is assumed to be caused by an energy gradient in between the confinement and the Rindler zone and its equation is derived directly from the uncertainty principle. Discharging capacitors with various thicknesses are compared and show agreement between the experimental findings and a virtual particle oscillation associated with a standing wave energy gradient hypothesis. The preliminary results are encouraging.

**Keywords:** electric propulsion, Unruh radiation, Rindler Horizon, electron discharge thrust, quantum vacuum thruster, QVT, quantised inertia, imFAB, discrete virtual particle spectrum, quantum foam, information horizon energy gradient

## 1 Introduction

It was experimentally observed (Becker F.M. 1990) that a thinly charged parallel plate capacitor, supplied with high voltage values of 5 kV DC - 10 kV DC, exerted an unexpected observable force towards the anode. This anomaly was only detected while using dielectrics with low dielectric breakdown strength. However, it progressively disappeared when increasing the dielectric breakdown voltage (and the material thickness). Such phenomenon was initially disregarded as a likely artifact but a few years

later, additional considerations led to speculation that electric discharge could have been the cause of the anomaly. However, no further testing was conducted. The initial observations suggested that stronger dielectrics, with their enhanced performance in withstanding voltage, would not lead to an observable effect while the electric discharge (breakdown of insulation leading to partial/full discharge or field emission) could be responsible for the appearance of the phenomenon. In addition, Talley R.L. [11] had described a comparable anomalous observation which might have been caused by accelerating electrons or electric charges further reducing the likelihood of a simple artifact.

While conducting a variety of capacitive discharge experiments in 2017/2018 and additional battery powered wireless experiments in 2019, data was collected during field emission and insulation breakdown discharge events of parallel capacitive charged plates. Data was collected for very short capacitor plate distances. Additionally, the collected data investigated correlations between any anomalous force and the accelerated mass as well as any anomalous force with the reduction of the capacitor electrode distance, while keeping the accelerated mass constant.

## 2 Method

### Experimental setup and test apparatus

#### 2.1

Electrons are an easy-to-control option to achieve high acceleration of particles. Also, with reference to the anomalies characterized by Talley R.L. [11], such conditions are observed as potentially relevant. The high field strength achieved in a thin electrode separation can provide constant electron accelerations with a magnitude of  $10^{19}$  [m s<sup>-2</sup>] (where acceleration equals the fundamental electric charge divided by mass of an electron multiplied with voltage divided by the electrode distance  $a = \frac{Ve_e}{m_e d}$ ). This acceleration is associated directly to a Rindler horizon distance and a presumed maximum wavelength [8] in the spectrum of Unruh radiation. This is done by considering only the allowed radiation with nodes at the boundaries [7] which are able to be attenuated by the conductive plates within the range of normal engineering practices. The strong electric field releases electrons through the high-field emission effect [5]. With the objective of achieving higher force values, the material was heated so that the energy value required by the electric field for electron transmission could be lowered [9] (Schottky effect): in other words, warming the material allowed an increase in the discharge of electrons using the same electric field strength. The application of heat enables thermionic emission as well as supplying some electrons with at least the minimal energy required to overcome the barrier force holding them in the material structure (reference to the concept of work functions of materials).

#### 2.2

Capacitors were designed with polyethylene dielectric materials. Other materials, such as paper, glycerin, and porous plastics, were also tested but this resulted in discharges involving ionic charge flow which traveled in the opposite direction of the electron flow, hindering the effect. Furthermore, some materials were prone to cavities (atmospheric voids) that introduced partial discharges [3] where electron avalanches

generated ion current contribution inside the hollow space. Additionally, paper insulators were ineffective in generating measurable thrust effects since the atmospheric electron avalanches (see Paschen law [2] for breakdown voltage vs distance) would release secondary electrons but also induce ionization as well. Overall the experimental data seem to validate that for the design and manufacturing of a thruster device using the observed phenomenon, a vacuum propagation of the accelerated electrons or the application of semiconductor cathode arrays could be the most effective method to obtain a controllable effect.

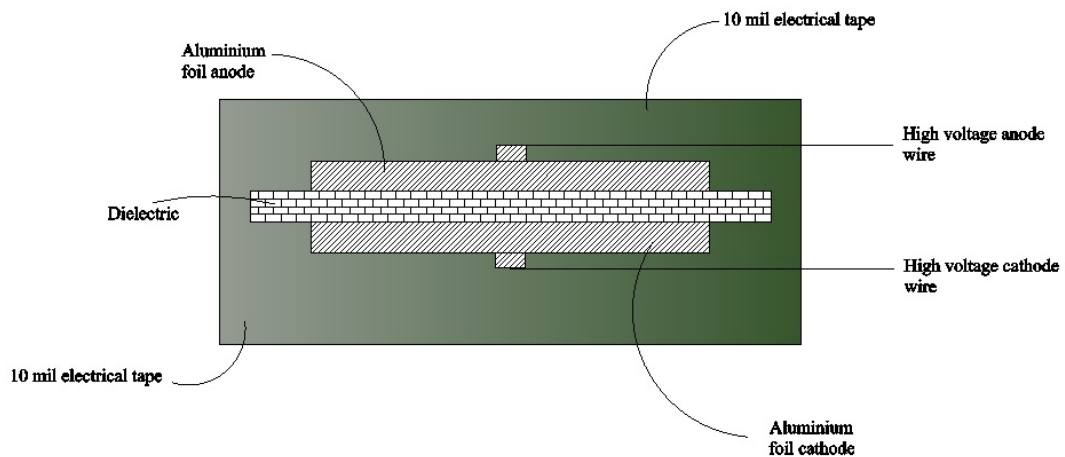


Figure 1: General prototype construction

Remark: Depending on the actual insulator thickness it can be assumed that currents slightly below  $1 \mu\text{A}$  are essential to generate thrust forces to trigger the load sensor (i.e. LEADZM B3003T digital scale with typical sensitivity of 0.001 g and error of 0.003 g). Additionally, a new Adam LPB 623i scale was used in 2021 tests with a 0.001 g sensitivity and 0.002 g error. Adam scale 623i also has a built in center of gravity feature as well as internal calibration.

Considering the available power sources (5 kV DC, 10 kV DC), the electric field strength between the capacitor plates was estimated to be below the actual effective tunneling field strength required to provide a sufficiently reliable current density to support the effect [15] [16]. Therefore, the homogeneous field character had to be enhanced into a partial inhomogeneous field to increase the field strength by altering the smooth flat shape of the emitting surface by adding sharper edges. This reduced the radius of the emitting surface which increased the electric field strength similar to the concept of a needle cathode. This was done by cutting into the electrode or by using sandpaper on the cathode surface to facilitate field emission. This was done using a precision knife by applying a high number (hundreds) of small cuts on the electrode or by surface treatment with a fine sandpaper. Obtaining a sharp edge contributes to

a higher field strength through the creation of inhomogeneous electric fields similar to a needle electrode. If only homogenous fields were used, this cold emission would need an electric field strength to begin on the order around  $10^7$  to  $10^8$  [V/m].

For some tests typically associated with higher thrust force values, the overall capacitor was preheated up to approximately  $50$  °C before placing the device onto the measurement apparatus. This also denoted that testing attempts at low ambient temperatures without pre-heating could lead to a thrust force too low to be detected. Verification tests had been conducted to evaluate the setup against unwanted external influences like ionic wind. Before testing a control capacitor was used as a test sample. These control capacitors, as well as the supply conductors, were supplied with a same or higher voltage level than the actual force cell. The control capacitors used were of equivalent design but insulation dielectric had a higher dielectric strength. Additionally, an increased insulation thickness between the plates were used to prevent current discharge (absence of field emission). The verification testing of this control capacitor setup resulted in a zero force measurement . Furthermore, a control resistor circuit (in place of control capacitor) had been utilized to run a larger current than the typical field emission current through the system to demonstrate this had no effect on the observable force measurement.

### 2.3

Confirmation tests in soft vacuum were conducted by placing the capacitor inside a sealed container, shielded by wrapping it in a conductive grounded outer layer. Such tests yielded results comparable, in terms of average, with the open air set-up. However, the corresponding spread standard deviation of the data points recorded was lower for the soft vacuum ( $\sim 20$  torr) during experimental tests.

### 2.4

The supply wires had been twisted [1] to reduce electromagnetic effects (Lorentz force etc.). This operation was performed very carefully to prevent the generation of torque onto the system. Nevertheless, the order of magnitude of theoretical torque contribution was estimated to be sufficiently low to not alter the observable phenomenon thus reducing concerns related to any possible residual torque. Moreover, the supply conductors were routed an adequate distance ( $\sim 200$  mm) to prevent electromagnetic field disturbances on the load cell of the digital scale. Field disturbances to the load cell leading to the corruption of displayed measurements were observed in a range of less than  $\sim 50$  mm around the digital scale. The metal film shunt resistors used for voltage measurements to determine the electric current had a 1 % error tolerance while the probes used were approximately 2 %. The scope used for electric current measurements was a Keysight DSO1052B Oscilloscope-2 Channel-50 MHz.

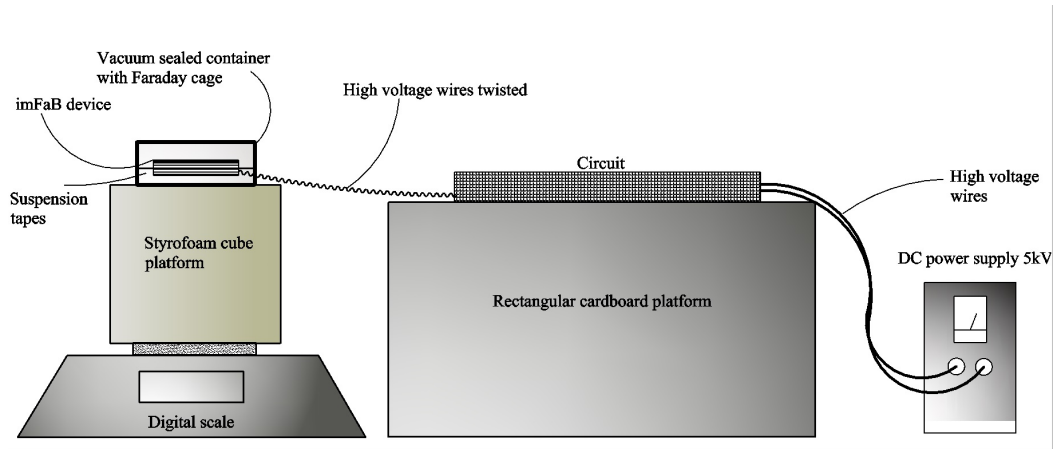


Figure 2: Experiment setup

## 2.5

The dielectrics had been tightly fit between the conductive surfaces to minimize air presence. If a considerable air layer was present, this could have led to ions traveling in the opposite direction of the electrons due to avalanche processes by direct arcing which would dampen the amplitude of observed thrust. As previously explained, this might also occur in certain materials when the high-field strength introduces partial internal discharges in material porosities where electrons as well as secondary avalanche electrons can generate positive charged ions. Furthermore, when glow-discharge/stronger arcing occurred, the acceleration voltage over the capacitor would decrease significantly, down to a typical  $\sim 30V$  arc voltage level. In this condition, particles, instead of being linearly accelerated, would be subject to Langmuir waves: rapid plasma oscillations of electron density related to the instability in the dielectric function. These occurrences were noted to occur occasionally with the test device accelerating slightly towards the earth regardless of the polarity. Consequently, the experiment was set up to minimize the risk of these occurrences. Furthermore it had been observed that utilizing significantly thinner dielectric insulators would result in the observation of peaks in the measured discharge electric current waveform. By wave form these appear to be associated to partial discharge events (e.g. ion tail characteristics) and should be disregarded for a clean measurement setup due to the effect that the positive ions during partial discharge event inside the material voids would accelerate in the opposite direction of the electrons. A force effect may establish with this condition, however the force would be diluted and therefore the thrust force would not follow the prediction. Such events might arise when using very thin Kapton as insulator. Identification would involve using an oscilloscope and one should review the typical partial discharge onset voltages as low as 500 to 800V. One should note, partial discharges would degrade the dielectric and therefore might not be practical in real life applications.

## 2.6

It was essential to protect the measurement tools/devices of the circuit from the influences of voltage transients that could occur in a situation where the insulation resistance of the capacitor would drop significantly. In such cases, the shunt resistor would carry a higher voltage due to the voltage divider characteristic of the circuit (more precisely, this is related to the capacitor insulator experiencing a reduced resistance). The circuit, see Fig. 3, did not employ any preventive measures for such phenomena. However a series connected large resistor, with respect to the shunt resistive value, could be introduced to serve as a voltage divider in case of insulation failure. Such transient effects are seen more likely when the field emission current increases. In addition, heating the dielectric insulation material could potentially reduce the insulation resistance of the dielectrics.

## 2.7

An alternative to the 5 kV DC commercial power source was also used. A conventional flyback transformer with a maximum output slightly above 10 kV DC had been utilized for voltage sweeping during the experiments to vary the electron's acceleration. The flyback transformer was supplied in the primary winding by a conventional DC power supply. The output voltage characteristic has been interpolated by the input/output data specifications of the flyback manufacturer for computations. Additionally, the electric circuit was rectified (smoothed) by a tank capacitor to provide a stable supply voltage to the capacitor. For the testing in 2021, an EMCO 4kV power supply had been used. (for onboard testing; see chapter 2.8 for further details)

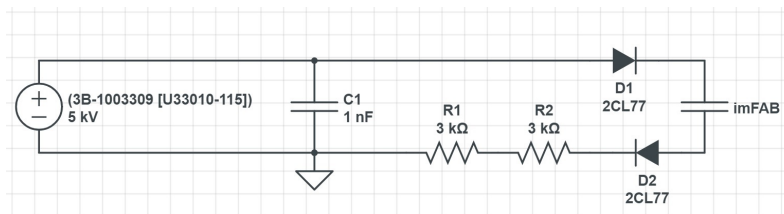


Figure 3: Functional circuit

## 2.8 Wireless Setup

During additional testing in January 2019, the entire thruster system was placed inside a grounded faraday cage with an inner insulation barrier. Only DC supply wires exited the cage and were connected to a battery-onboard. These low voltage DC supply wires ran vertically and twisted until terminal connections at the flyback transformer. All high voltage components were located inside the cage without any atmospheric exposed HV supply conductors. The thruster box, including the battery power supply and high voltage source, was placed on the scale and the center of gravity effects were addressed before measurement. Additionally, a wireless relay was installed on the top of the cage to turn the system on and off remotely without physical access. Signal

conductors were routed to the measurement circuit (shunt to the oscilloscope). The effect device ON voltage level was fixed to around 5kV. This was measured from the output of the flyback transformer with a smoothing capacitor in parallel. Finally, additional verification testing in 2021 was done. (see Appendix for force time charts)

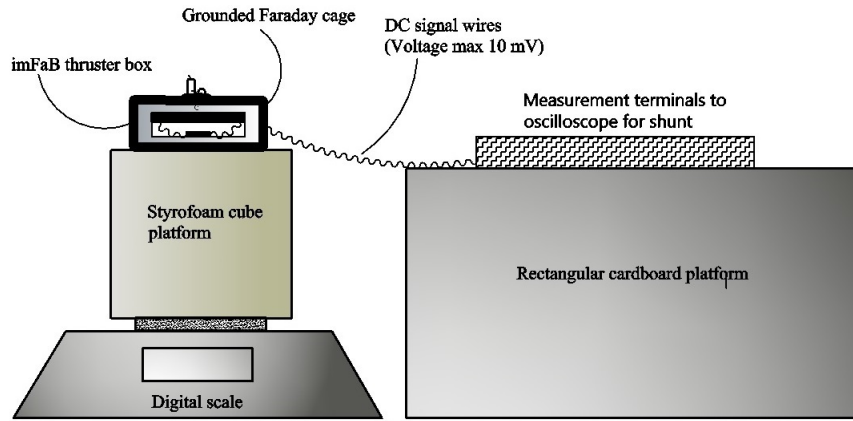


Figure 4: Wireless setup

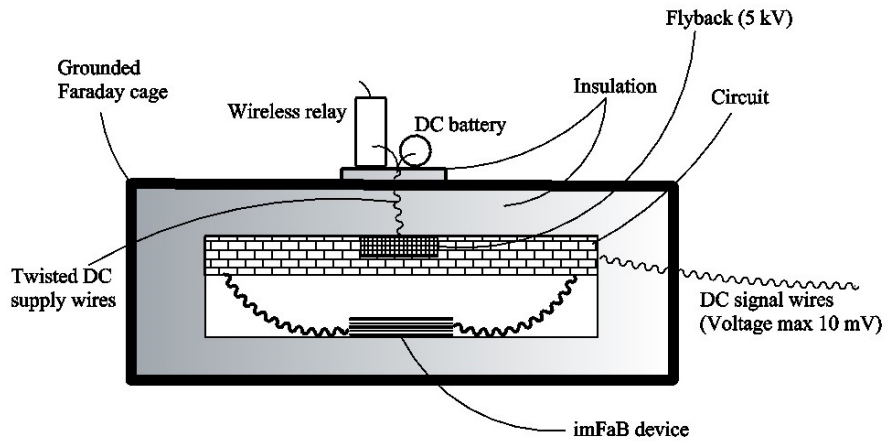


Figure 5: Thruster device

## 3 Results

### 3.1 Thrust observation versus electrode distances

The electrode distance had been varied and the force monitored. Since the discharge current is dependent on the Schottky effect (field enhanced thermionic emission), which is determined not only by the electric field strength but also by the heat of the surface, the actual current for each data point statistically fluctuates. Consequently the graphs showing the results of the current measurements are normalized (same charge amount, same accelerated mass). These explained predictions also might correlate to a proposed hypothetical model of a quantum oscillator and/or a zero point field spectrum oscillation which provide a discrete spectrum where Unruh radiation is generated by a Rindler information boundary horizon caused by acceleration of electrons.

Note: accelerated accumulated mass corresponds in value to the electric current multiplied with the mass of an electron and divided by the elementary charge.

If a constant current (an accelerated mass of electrons) is provided, the reduction of the distance between the electrodes cause the thrust force effect to exponentially increase in value. The electrodes distance is equivalent to the dielectric insulation thickness and in the remainder of the paper the two dimensional characteristics are used interchangeably being equal in value.

The first sub-experiment was conducted with different insulator thicknesses between  $13 \mu\text{m}$  to  $80 \mu\text{m}$ . These different thicknesses influenced the acceleration experienced by the electrons. The diameters of the capacitors ranged from  $2.5 \mu\text{m}$  to  $5 \mu\text{m}$  and a total of 266 data points were collected. The measured current value was standardized (due to fluctuation under the effect of field emission) to a normalized current level of an arbitrary  $10 \mu\text{A}$ . The accelerated voltage was tuned to 5 kV for all measurement points while testing different insulation thicknesses. The acceleration voltage of approximately 5 kV corresponds to an electric acceleration inside the insulator thicknesses on the order of  $10^{18}$  to  $10^{19} [\text{m s}^{-2}]$ .

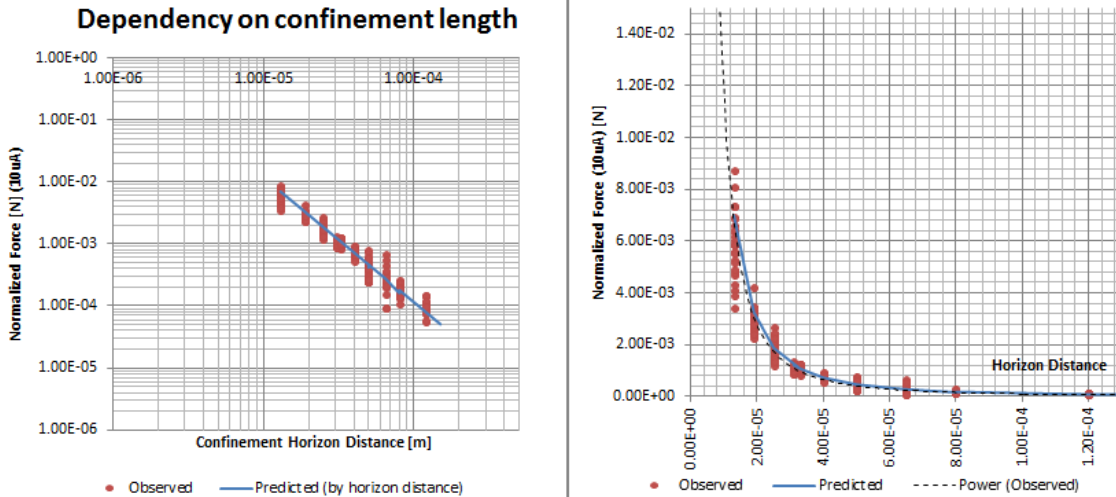


Figure 6: Normalized force versus distance

While altering the electrode’s distance, it is observed that the recorded force follows a linear trend in a logarithmic view. Hence the trend is attributed to an exponential increase of force by a linear reduction of the electrodes distance. Later, this will be defined as a horizon distance or confinement of the seeing zone; an expression is used by McCulloch relating to the propagation direction. This zone is located in front of the accelerating particle.

Unless otherwise specified, data points of individual graphs are considered to be an absolute value since the data points correspond to both directional scenarios (a force towards and opposite the measurement scale). The anode of the capacitor pointing upwards was associated to an upward acceleration while the anode pointing downwards was associated to a downward acceleration. This remained valid as long as no reversal force mechanism was introduced (see section 3.3 for details).

In Fig. 7, the actual force direction shows dependency on the measured accelerated mass derived from the proportional electric current. The symmetry of the data points illustrates that the observed force appears independent of influences of gravity, ionic winds, thermal buoyancy and other such artifacts. Additionally, several tests have been conducted in a low vacuum using a simple sealed container (data points identified as ‘vac’ in the attached graph), showing a trend line characterized by a lower standard deviation compared to the open-air tests. The top half of graph, where the force is positive, corresponds to the anode facing upwards while the bottom portion corresponds to the anode facing downwards.

Note: Vacuum measurements from the median thrust observations (conducted on the 33  $\mu\text{m}$  capacitor) are associated to a 8 % standard deviation. Other non-vacuum measurements are in the range from 11 % (33  $\mu\text{m}$ ) to higher values of 30 % (50  $\mu\text{m}$ ). The vacuum appears to have a stabilizing effect from 12 % ( $\sigma = 1.2 * 10^{-4}$  N at mean of  $1.0 * 10^{-3}$  N) down to 8 % ( $\sigma = 8.7 * 10^{-5}$  N at mean of  $1.1 * 10^{-3}$  N).

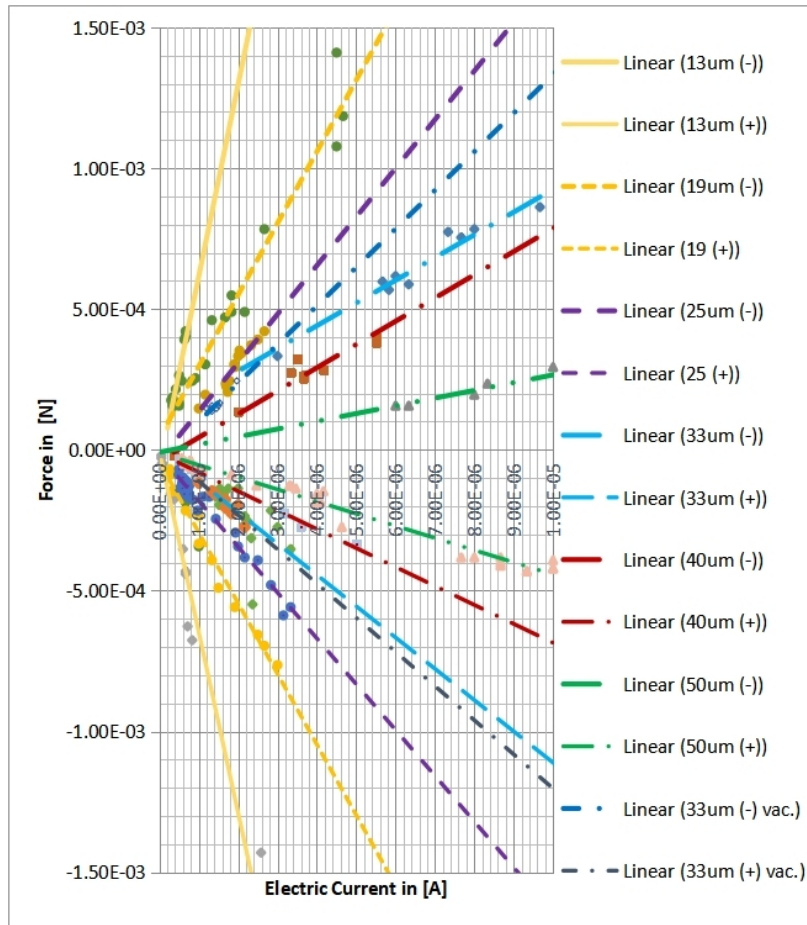


Figure 7: Force versus Current

The operational characteristic of the identified thrust effect shows a linear dependency on the amount of accelerated electron mass and increases exponentially with a linear decrease of electrode distance.

**Note:** The graph shows that for thicker insulators the observed thrust was greater when the anode (+) was oriented up as the top of the capacitor. This fact could be correlated with a slight influence of buoyancy determined by the preheating which is required to obtain higher force values.

Furthermore, the capacitor plates were tested in vertical position in the attempt to have a null effect which would confirm the absence of external perturbations. This verification test was also conducted obtaining a null force. Namely, a force vector and the thrust readings were observed as not being diffuse which confirmed the validity of the experimental set-up and the directional attribute of the thrust.

The graph hereunder shows similar trend lines with respect to the estimated power consumption.

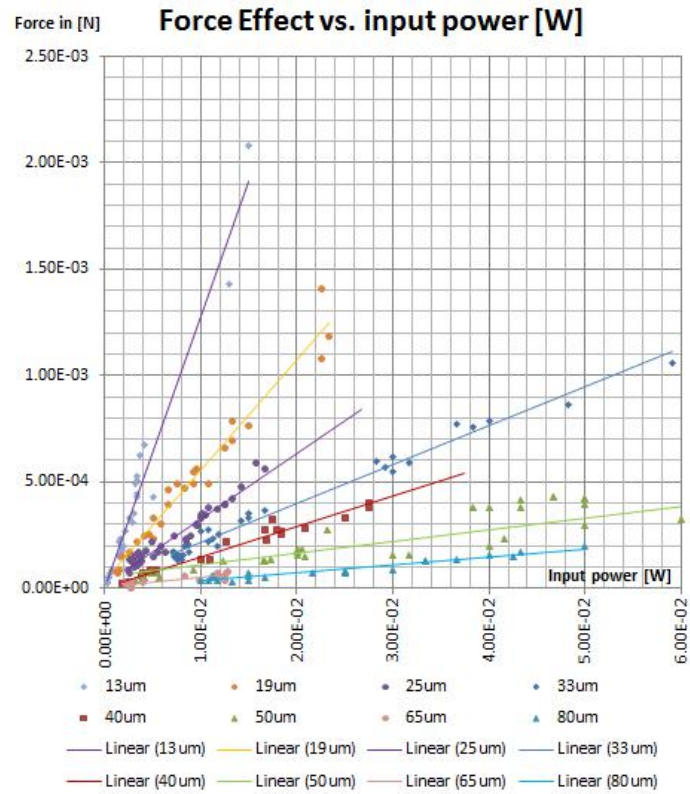


Figure 8: Force versus input power

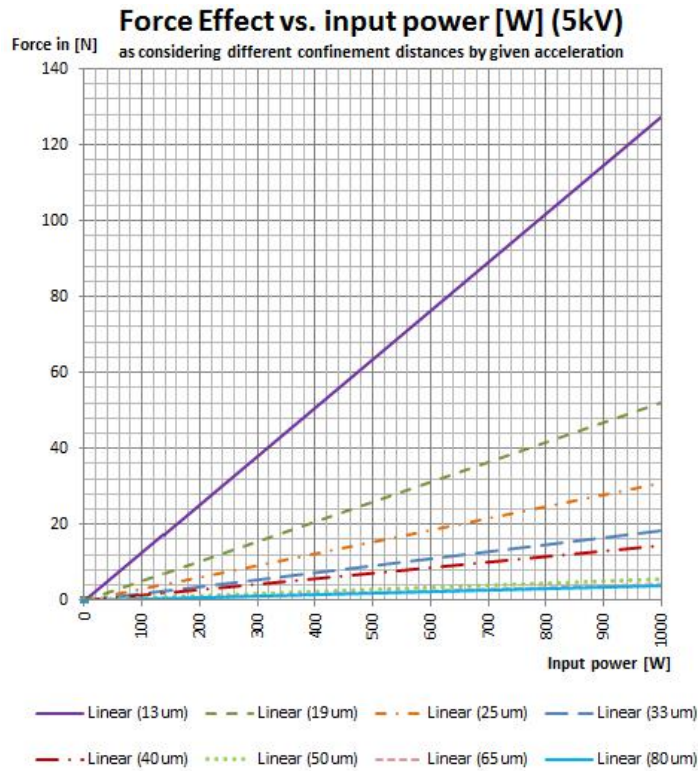


Figure 9: Force versus input power extrapolated

The same graph can be extrapolated to show the force versus power ratio of a scaled up thruster device to 1 kW input power.

Remark: Lower thrust performance on thicker insulators is associated with a higher standard deviation as seen visible in the graph's lower left corner. Higher force values are associated with applied heat in conjunction with shorter electrode distances. From a practical perspective, this is important evidence because the output of a high thrust device should be easier to control.

Furthermore, the effect and operational thrust characteristics can be displayed by the combination of the square root of the accelerated mass and the energy gradient between the Unruh baths into one factor. The linearity on the logarithmic scale shows a combined dependency of the mass and Unruh radiation energy which is related to the accelerating particle.

**Note:** This view provides the advantage to compare all electrode separation distances in one combined graph.

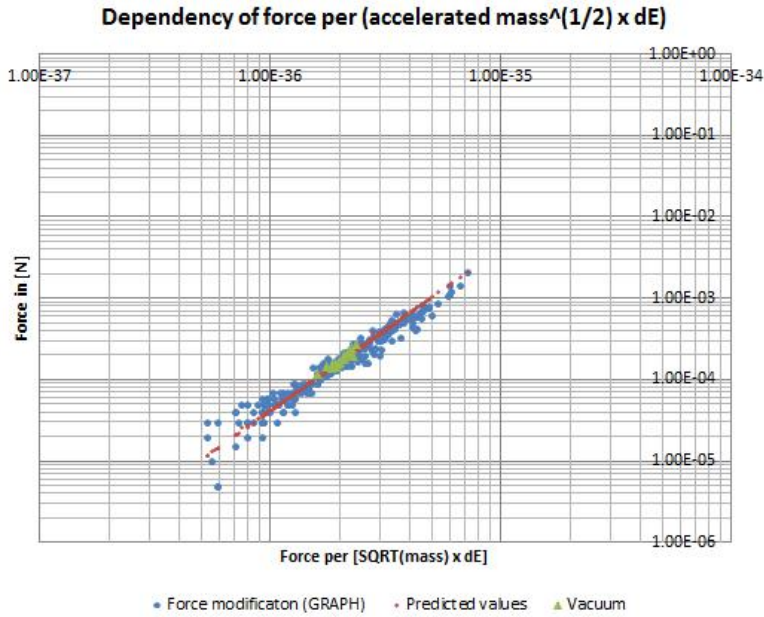


Figure 10: Force versus accelerated mass and energy

The use of the low vacuum container, where the thrust device is placed and shielded inside, appears to stabilize the measured data points versus prediction.

### 3.2 Thrust versus change of acceleration voltage as proportional to the Rindler distance

The Rindler distance is determined by the electric field strength and acceleration. Electric acceleration is yielded by the following: electric field strength multiplied by the elementary charge divided by electron mass  $a_e = Eq/m_e$ . Here the electric field strength is determined by voltage divided by electrode distances. In reference to the works of M.E. McCulloch, the Rindler distance had been calculated by the square of the speed of light divided by the acceleration  $R = c^2/a$  [6]. When the voltage supply remains connected during testing, the electric field strength will not be reduced by the dielectric constant of the insulation material. Only the stored charge  $Q$  of the system is increased. With an active source connected, the applied working voltage across the capacitor plates dictates the electric field strength and, therefore, the acceleration of the electrons. It should be noted that this is a different condition from the typical view from science literature explaining that the field strength is reduced after inserting dielectric inside a charged but not source connected capacitor. [19]

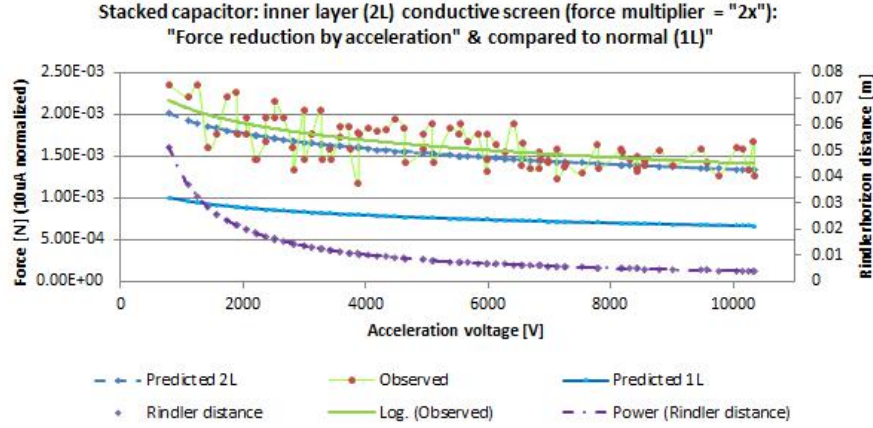


Figure 11: Force versus acceleration voltage for double layer capacitor

As voltage was increased, a slight decrease in normalized force occurred. Voltage was swept from 1 kV to approximately 10 kV and a total of 97 data points were collected. Furthermore, capacitor elements were stacked in series in an attempt to obtain a force multiplier factor. With respect to the reduction of the force with an increase in acceleration voltage, it is evident that an effect increase corresponds to the reciprocal of the accelerated electrons' kinetic energy. The effect is reduced with an increase in the particle's kinetic energy.

With respect to the measured force multiplication, a modified capacitor was used. This incorporated an additional inner conductive floating material similar to the cathode/anode foil in-between the two insulators. Such an arrangement represents a series capacitor where each voltage was approximately halved. Assuming that the supply current yielded the same volume of electrons, the results suggest that the electrons got accelerated twice. The prediction method, (see section 4) using the number of events for each accelerated particle, would only yield about half of the measured force value. Doubling the amount of events, since the electron gets re-accelerated from the inner floating plate, resulted in a prediction that would be in compliance with the observation.

It should be noted that by using the proposed physical model, a reduction of the Rindler distance compared to the confinement zone located in front of the accelerating particle, would reduce the number of unshared wavelengths. This, in-turn, would influence the energy gradient. This influence resulted in a decrease in  $dE$  which was the energy difference between the potentials of Rindler zone and propagation area.

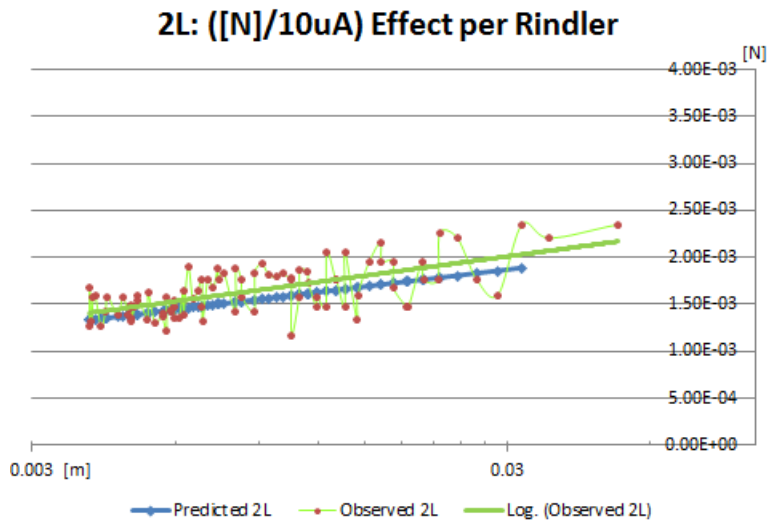


Figure 12: Force versus Rindler distance at  $10\mu A$

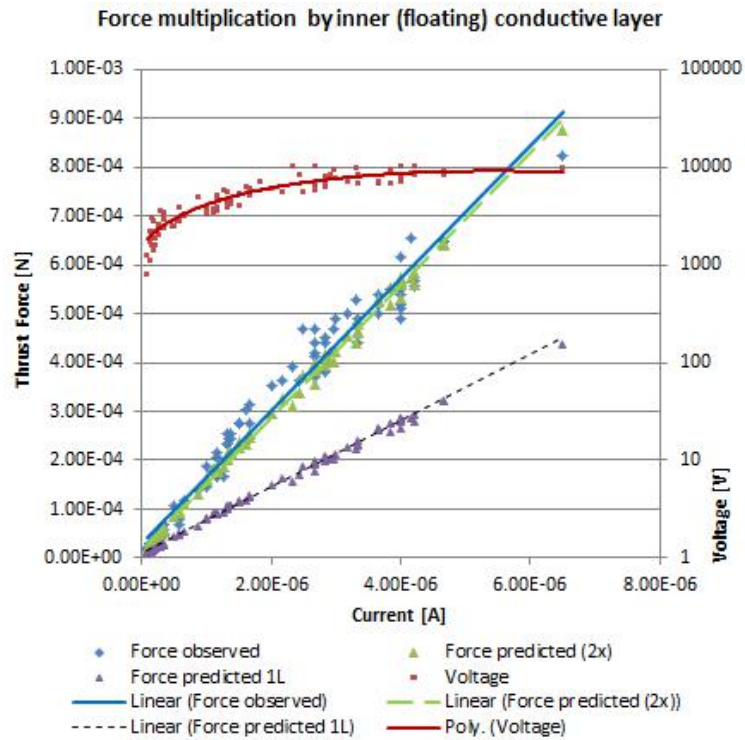


Figure 13: Force versus current for double layer capacitor

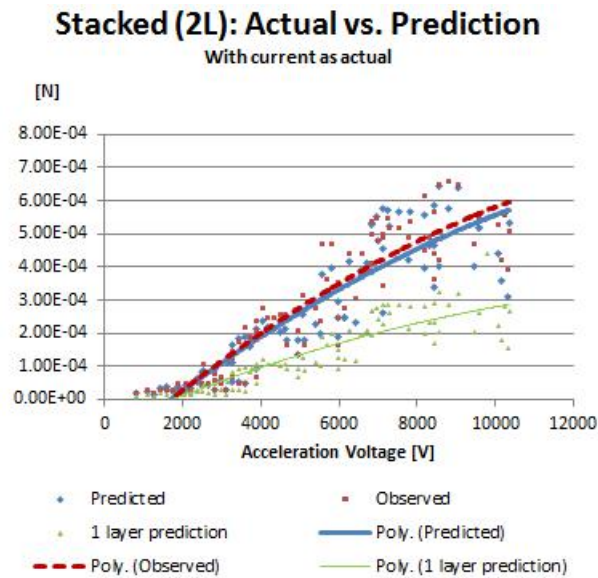


Figure 14: Force versus voltage for double layer capacitor

For reference, Fig. 15 illustrates the overall weight modification observed during the various experiments.

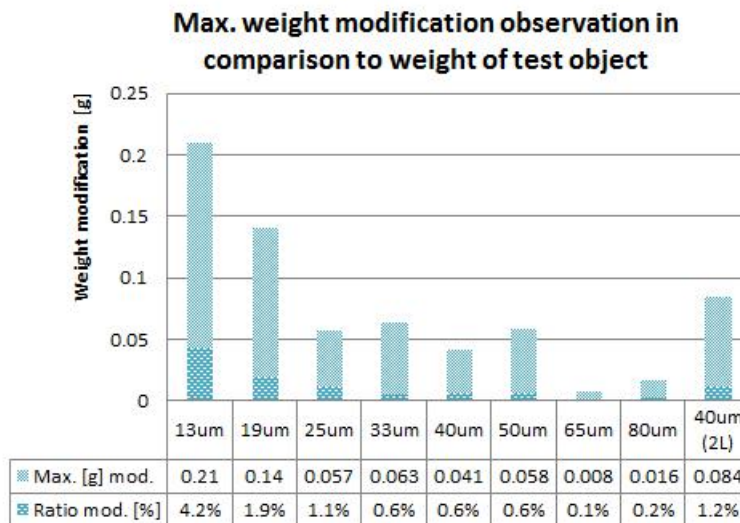


Figure 15: Maximum weight modification for all capacitors

An interesting piece of evidence was that some capacitors showed a lower performance with a lower number of accelerated particles: such performance was detected by mea-

suring a lower electric current. The main purpose of this figure is to show the highest amount of force achieved using different electrodes distances.

### 3.3 Altering Rindler zone with insertion of conductive attenuated materials

Additional tests performed (144 data points) resulted in the identification of a directional force reversal. When a particle or object is accelerated, a Rindler horizon forms behind it. Therefore, assuming the existence of this information boundary zone, an experiment had been conducted by inserting a conductive material into this zone. According to the skin depth's equation (see Appendix B), it is assumed that even a thin material could attenuate up to the maximum wavelength of the standing waves where nodes reside at the horizon as allowed by the Rindler distance.

Four different behaviors were identified:

1. When the thickness of the cathode was extended before the rindler horizon,  $R$ , the thrust effect appeared to be linearly reduced (slope of  $-2R$ ) with respect to the cathode elongation.
2. When a conductive material, electrically insulated from the cathode, was inserted into a certain area behind the cathode but before  $R$ , a full force reversal was observed compared to the original observed effect.
3. When a conductive material, electrically insulated from the cathode, was inserted a sufficient distance behind the cathode and beyond  $R$ , a normal effect was observed.
4. When the cathode thickness was extended beyond  $R$ , a full force reversal was observed compared to the original observed effect.

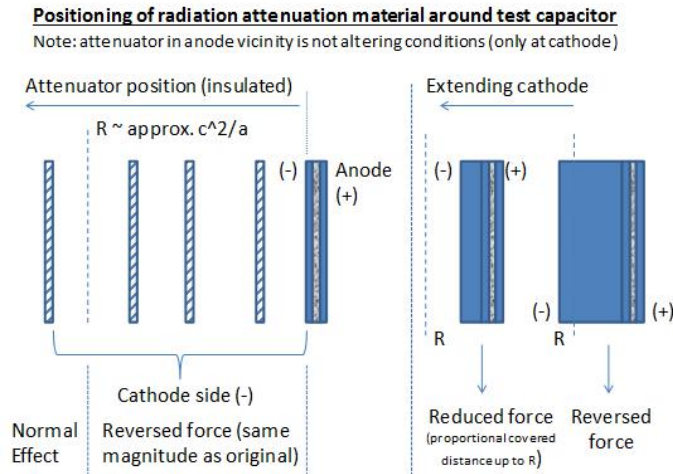


Figure 16: Strategic positioning of radiation attenuation materials

Suspecting that the forces observed are linked to the quantum field radiation experienced by the capacitor during the electrons acceleration, several additional tests were performed in an attempt to dampen shorter wavelengths thus influencing the generated force. This was done introducing an attenuation material, aluminium sheet on the order of a few tenths of a millimeter, at several distances from the cathode surface.

After numerous tests, it was discovered that the force could be reversed with same value of the original force at all distances less than the rindler horizon  $R$  when the attenuation material was electrically insulated from the cathode. When placing the attenuator past  $R$  (a length approximately equal  $c^2/a$ ), a sudden change of force direction occurred. This change in direction with the attenuator sheet the beyond the rindler horizon led to the sudden recovery of the original force direction (towards the anode aligned to electron propagation path).

Furthermore it was observed that an extension in the conducting cathode thickness did not lead to a force reversal but to a reduction of force. This was estimated as being proportional to the covered space between original position of the cathode surface and the rindler distance,  $R$ . It should also be noted that there could be an exponential decrease since data points between 0 and  $R$ . Finally, if the cathode thickness exceeded  $R$  a force reversal was established with the same magnitude of the full normal effect: propagation toward the anode.

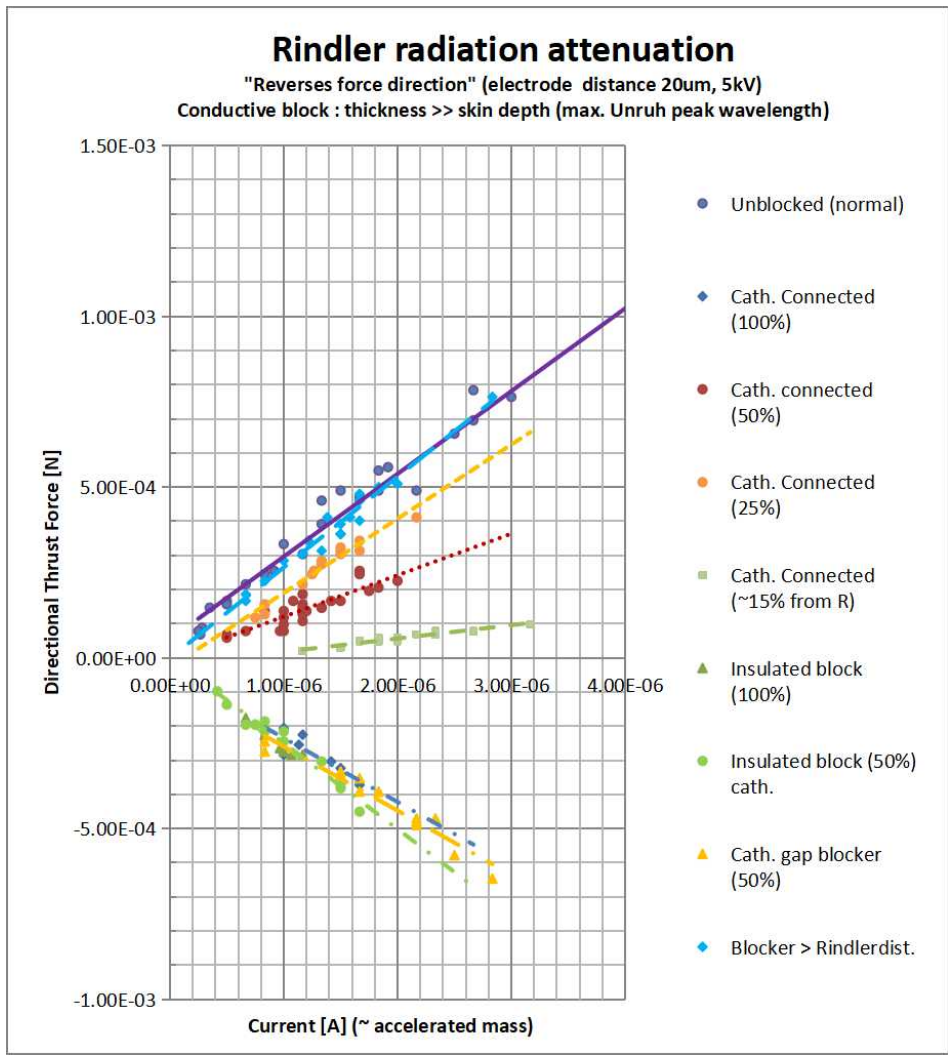


Figure 17: Force [N] versus current for various blockers

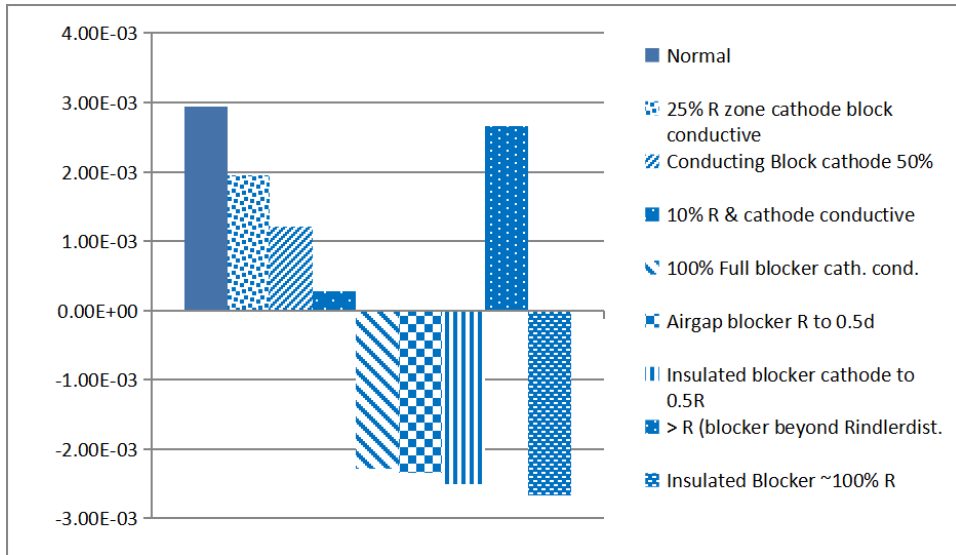


Figure 18: Force [N] for different blockers with data measurements averaged

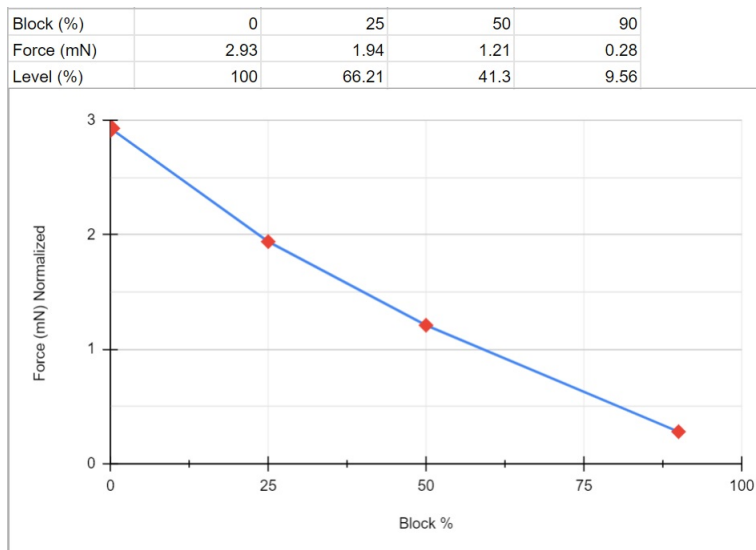


Figure 19: Force [N] reduction for blockers with data measurements averaged

The observation an accelerated direction reversal, with same level of the original thrust force, might be seen as an effect involving an accelerated frame of reference. During the original effect, the Rindler horizon propagated together with the electrically accelerated electron (co-moving) and the Rindler horizon moved as the electron traveled.

Looking into this specific scenario it can be considered to be one accelerated inertial reference frame which is initially accelerated at the same level of the electric acceleration. Physical standard models describe this accelerated situation by introducing one fictitious/pseudo force (adding an electrical acceleration force vector) which denotes an additional thrust acceleration vector. As per Newton's third law, forces only exist in pairs and this inertial force on the electron's co-moving inertial accelerated frame could be assumed to be directed opposite to the accelerated direction of electron propagation. In the frame of the external observer, this fictitious/pseudo force could change the acceleration direction since the actual effect force is cancelled by the causal blocking of the Rindler horizon. In this model the other pair component of the cancelled pseudo force would remain valid and directs the acceleration direction leading to a reversal. This might happen because the energy of Rindler zone could be assumed to stay present/valid, but is not able to propagate to provide an accelerative force; hence, the inertial force pair stays in existence. Further research is suggested on this simplified model in order to compute both the amplitude of the force and to identify the causation relevant to the conductive blocker conditions.

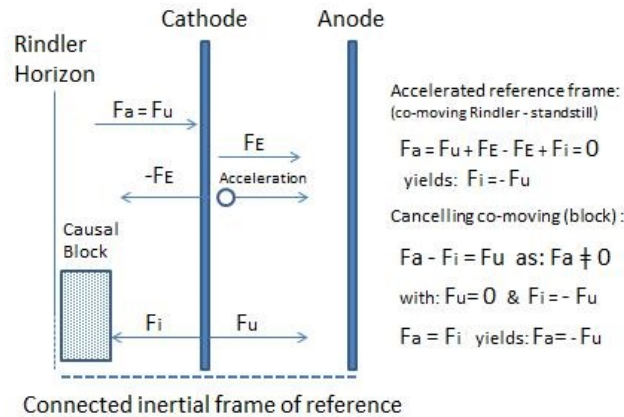


Figure 20: Inertial frame force

### 3.4 Wireless Experimental Results

The new battery-powered onboard wireless setup resulted in a convergent force trendline with the previous data collected for 20  $\mu\text{m}$  distance (October 2018). Both devices had a supplied voltage of 5 kV. Generally, smaller thrust values from lower current were found due to lower ambient temperature conditions and lack of heat applied to the imFAB device. When using a battery supply in conjunction with a flyback transformer or similar circuit for a high voltage source, it is recommended to use a tank capacitor in parallel to the low voltage DC battery output to attempt to compensate for the pulsing load condition in the primary supply circuit which could affect the battery performance. Applied heating to increase electric current was avoided to prevent heat trapped inside the closed grounded Faraday cage. This could have resulted in buoyancy errors. Also, additional testing was performed in 2021 confirming positive

thrust observations.

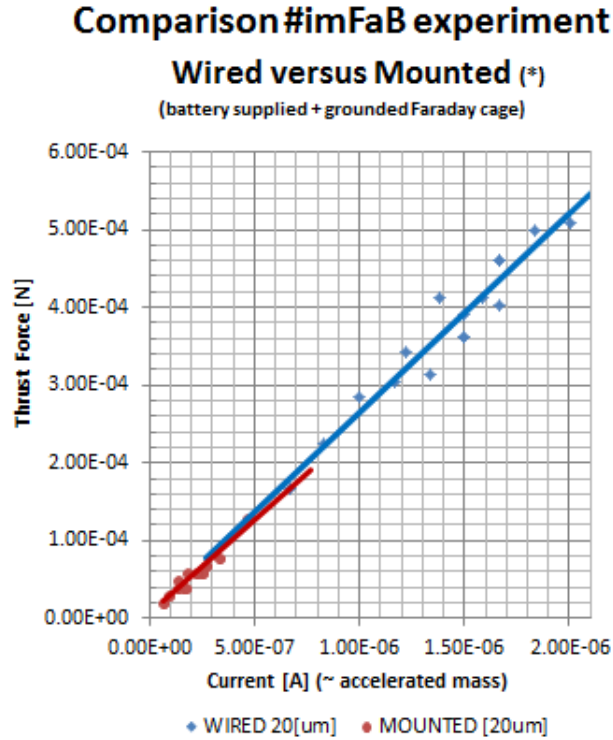


Figure 21: Wireless

## 4 Method

In particular the fast/frequent burst electric discharge thrust effect (named FBeDT) is not only associated to capacitors, where the thrust towards the anode is caused by the effects from the high voltage supply [10], but is a more general effect that uses capacitors as an experimental mechanism to accelerate particles in a defined accelerated condition. The electric acceleration is used to observe an effect caused by propagating electric charges. In particular, electrons discharged during insulation breakdown and field emission tunneling within solid materials with very high electric field result in hyper-accelerating electrons. Additionally, the thrust effect is reversible not only by changing polarity (reversing the acceleration direction), but by altering conditions in the space behind the accelerated electrons, namely, between the Rindler horizon and the cathode. The capacitors are used as a mechanism to accelerate particles with a known particle mass and can be achieved using very short electrode distances.

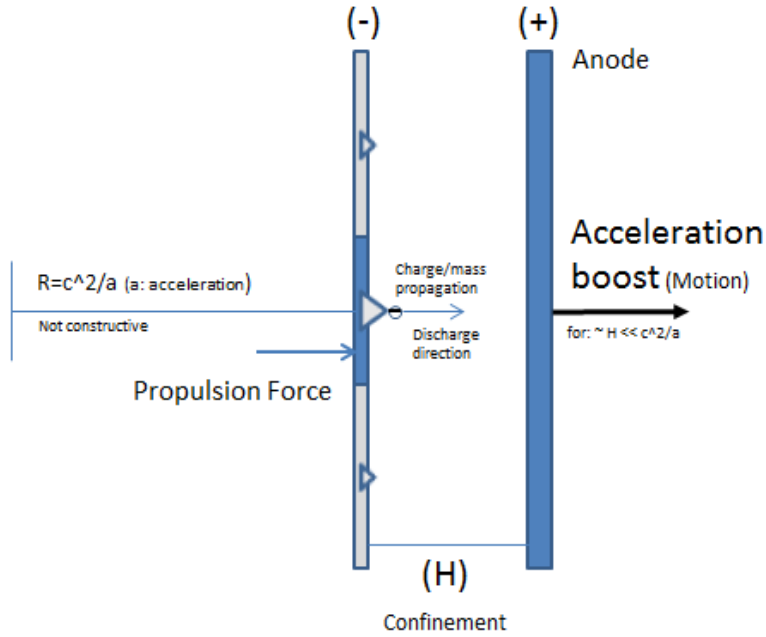


Figure 22: Force diagram of thruster

According to the latest understandings in physics, it is probable that both singularity horizons [4] and Rindler horizons generate thermal radiation [12] [13]. Recent developments in theoretical physics [7] [8] assume such radiation to be confined within boundaries and could be quantised with wave nodes at the horizons. Under normal conditions an accelerated particle experiences a maximum thermal Unruh radiation (peak wavelength) of approximately 8 times the maximum wavelength in the Rindler horizon zone. This situation causes inertia [7] [8].

To alter the inertia of an object, it is assumed that it would be possible to reduce the maximum Unruh wavelength, or equivalent associated harmonic oscillations, by virtual particles. This could be established by information loss at a horizon in the region in front of an accelerating object. Therefore this reduces the discrete, due to nodes at the horizon, spectrum and the total amount of waves allowed in the confinement. In a confinement condition, wave attenuation would be accomplished by reducing the distance to the information boundary and would limit the maximum radiation wavelength in front of the accelerated object and the Rindler horizon. If a confinement in the electron propagation path is established and is equivalent to the distance of the Rindler horizon, an inertia equilibrium situation would be achieved. If the attenuation position is further reduced, more Unruh waves in the propagation zone would be cancelled and the total wave energy (in the zero point field) in front of the accelerating particle would be less available in this horizon zone. In the case of small particles, this would allow a one dimensional methodology to simulate the conditions.

## 4.1 Theoretical force model by uncertainty principle

Having documented and demonstrated that an effect exists to generate an anomalous force, the question remains whether this could also work in theory. Begin by using the uncertainty principle  $\Delta x \Delta p = \hbar/2$  and the assumption that there are nodes at the horizons. The energy level is fully determined so  $\Delta x$  would be equivalent to the maximum possible uncertainty in the given boundaries (horizons).

Assuming that in a confined space  $\Delta x \Delta p = \hbar/2$  the confined attenuated energy is  $\Delta E$ , this would result in the summation of the total number of virtual particle oscillation energies down to the Planck length ( $l_p$ ). The linear momentum ( $\Delta p$ ) is equivalent and determined as  $\Delta E = \Delta pc$ .

Use the energy formula for a photon  $\Delta E = \Delta pc$  and substitute in for  $\Delta p = \frac{\hbar}{2\Delta x}$ .

$$\Delta E = \frac{\hbar c}{2\Delta x} \quad (1)$$

Here the unshared waves from the energy gradient will create a net force on the capacitor. This is due to the fact that the unshared waves only fit at the nodes of the rindler horizon and the cathode. The shared waves in both the Rindler region,  $R$ , and the confinement,  $d$ , will not attribute to any net force.

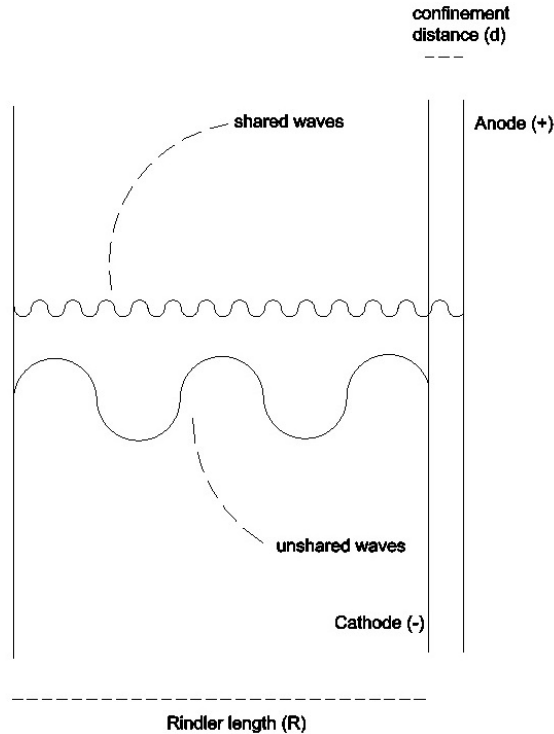


Figure 23: Unshared waves gradient force on capacitor

Plug in for  $\Delta x = kl_p$  in order to count all the waves in the confinement region up to  $N$ . Here  $l_p$  is denoted as Planck length. Additionally,  $N$  represents the number of the fundamental oscillations allowed in the confinement.

$$\sum_{k=1}^N \Delta E_d = \frac{\hbar c}{2l_p} + \frac{\hbar c}{4l_p} + \cdots + \frac{\hbar c}{2Nl_p} \quad (2)$$

Plug in for  $\Delta x = kl_p$  in order to count all the waves in the Rindler region distance ( $R$ ) up to  $M$ .

$$\sum_{k=1}^M \Delta E_R = \frac{\hbar c}{2l_p} + \frac{\hbar c}{4l_p} + \cdots + \frac{\hbar c}{2Ml_p} \quad (3)$$

Now compute the ratio of fractional energy that will be pushing the capacitor. Namely, the ratio  $\frac{\Delta E_R - \Delta E_d}{E_R}$ .

$$\frac{\Delta E_R - \Delta E_d}{\Delta E_R} = \left( \frac{\frac{\hbar c}{2l_p} + \frac{\hbar c}{4l_p} + \cdots + \frac{\hbar c}{2Ml_p}}{\frac{\hbar c}{2l_p} + \frac{\hbar c}{4l_p} + \cdots + \frac{\hbar c}{2Ml_p}} - \left( \frac{\hbar c}{2l_p} + \frac{\hbar c}{4l_p} + \cdots + \frac{\hbar c}{2Nl_p} \right) \right) \quad (4)$$

Now write the equation in closed form and simplify.

$$\frac{\Delta E_R - \Delta E_d}{\Delta E_R} = \frac{\sum_{k=1}^M \frac{1}{k} - \sum_{k=1}^N \frac{1}{k}}{\sum_{k=1}^M \frac{1}{k}} \quad (5)$$

Now, replace  $M$  with the total waves in the region  $R/l_p - 1$  which are the total waves in the Rindler region down to Planck length. Also replace  $N$  with  $d/l_p - 1$  which are the total waves in the confinement region. Finally, multiply by  $\frac{\hbar c}{2 \cdot 0.5d}$  using (1) to get the total energy gradient of one electron.

$$\Delta E_e = \frac{\hbar c}{d} \frac{\sum_{k=1}^{R/l_p-1} \frac{1}{k} - \sum_{k=1}^{d/l_p-1} \frac{1}{k}}{\sum_{k=1}^{R/l_p-1} \frac{1}{k}} \quad (6)$$

Use the closed form approximation for a harmonic series formula namely,  $\sum_{k=1}^N \frac{1}{k} \approx \ln \frac{2N+1}{2(1)-1}$  for both summations. This yields the same results as applying the Euler-Maclaurin formula for harmonic series, namely  $\sum_{k=1}^k \ln(k) + \gamma + \epsilon_k$  where  $\gamma$  is Euler's constant and  $\epsilon_k$  represents the higher order error terms.

$$\Delta E_e \approx \frac{\hbar c}{d} \frac{\ln\left(\frac{2R}{l_p}\right) - \ln\left(\frac{2d}{l_p}\right)}{\ln\left(\frac{2R}{l_p}\right)} \quad (7)$$

Fig. 24 suggests that a correlation with a physical action exists. The area under the curve represents [J m] which is the units of energy distance or action which is [kg m<sup>2</sup>s].

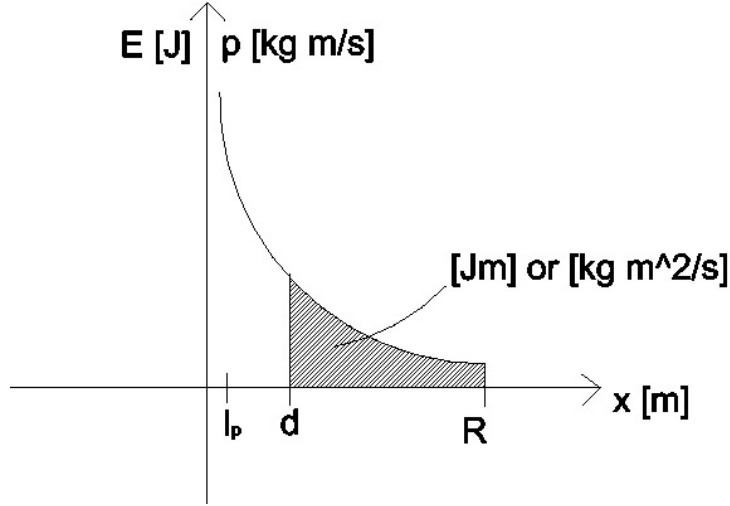


Figure 24: Energy and momentum versus distance

**Note:** Regarding Fig. 24 by conjugate variables, the linear momentum is the overall derivative of the corresponding action with respect to the position. In particular the uncertainty in position (also per quantum hydrodynamics) states that the action is the conjugate variable of the probability density.

Now also notice (7) can be written as the subtraction of two energy regions.

$$\Delta E_e \approx \frac{\hbar c}{d} \left( 1 - \frac{\ln(\frac{2d}{l_p})}{\ln(\frac{2R}{l_p})} \right) \quad (8)$$

Use the change of base formula to obtain the following. This results in the subtraction of two energy regions. Notice the full Rindler region is not used for  $\Delta x$ .

$$\Delta E_e \approx \frac{\hbar c}{d} \left( 1 - \log_{2R/l_p} 2d/l_p \right) \quad (9)$$

Now proceed back from (7) and combine the numerator using property of  $\ln a - \ln b = \ln(a/b)$  for a more simplistic form.

$$\Delta E_e \approx \frac{\hbar c}{d} \frac{\ln(\frac{R}{d})}{\ln(\frac{2R}{l_p})} \quad (10)$$

Now solve for the force  $\Delta F_e = \frac{\Delta E_e}{0.5d}$  by substituting in (8). Notice that this may suggest a centerpoint in the middle of the confinement distance might be relevant. This gradient was identified to be possible by measurement. This gradient might also denote a relation to the superimposed wave functions in a scenario where the average position of the Unruh radiation photons are in the middle of the confinement by Maupertuis's principle. Basically, the momentum of each harmonic oscillation is defined by its node from the information boundary: photons acting similar to an electron in a box scenario. The energy eigenstate has a symmetric probability amplitude, therefore, this

result leads to the notion that the uncertainty in position is distributed within the zone evenly, and henceforth, the average position is in the middle of the confinement. On the other hand, looking into a probabilistic density of the particles over the length of the confinement, one can see that an average low density level (like an energy divergence drain) would be statistically in the middle of a confinement. This might denote that the identified gradient is a probabilistic time averaged parameter. In another view, the double in energy could be associated to both the Rindler zone and confinement of electron zone within  $d$  superimposed. This paper will also highlight in the following pages other perspectives on this subject. Future additional research is suggested to find more clarity in the true nature in specific details of the presented models.

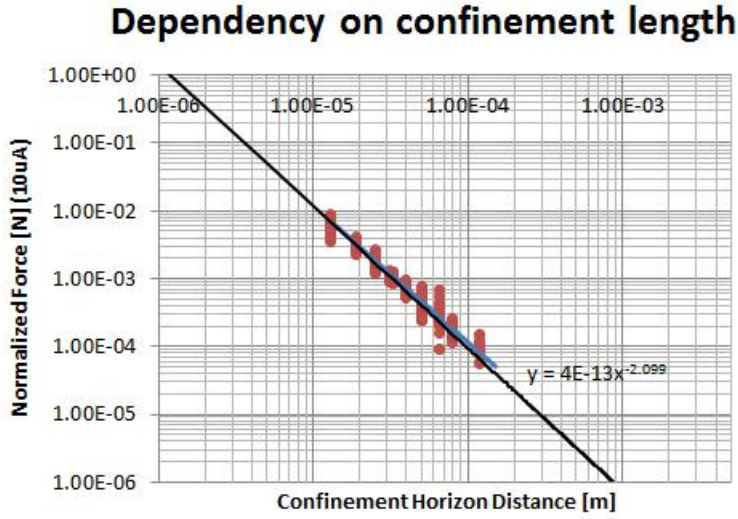


Figure 25: Normalized force versus confinement length

Take the derivation of the energy equation to obtain the following approximation using  $|F| = \frac{dE}{dx}$ .

$$\Delta F_e \approx \frac{\hbar c}{d^2} \frac{\ln(\frac{R}{d})}{\ln(\frac{2R}{l_p})} \quad (11)$$

The above results in the theoretical model for the force seen on one electron accelerated mass. Finally multiply by the number of electrons  $N_e$  to find the total force on the capacitor. This will need the accelerative events over one second. In this unit system one can count a one second flight duration over the current measured in ampere. Additionally, this might even indicate that an increase in current saturated in the one second time window on average could add a boost factor. Further experimental research is suggested to review a condition where the accumulated electron travel time over one second might exceed the normative one second duration which could boost the force amplitude.

$$\Delta F = \frac{\hbar c N_e}{d^2} \frac{\ln(\frac{R}{d})}{\ln(\frac{2R}{l_p})} \quad (12)$$

However, this is for a one dimensional system therefore all degrees of freedom need to be taken into account for this specific system.

$$h(x) = \cos\left(\frac{\pi x}{2R_{PH}}\right) \quad (13)$$

Now consider the nodes of the above function occurring at the two particle horizons and integrate the function to find the average value,  $\frac{1}{b-a} \int_a^b f(x) dx$ . In general the average value for any cosine function nodes at these positions will have this value. This represents the natural distribution of the virtual particles and the random average vector properties of the vacuum fluctuations.

$$H_{avg} = \frac{1}{R_{PH}} \int_0^{R_{PH}} \cos\left(\frac{\pi x}{2R_{PH}}\right) dx = \frac{4}{2\pi} \quad (14)$$

Then take the integral to account for all directions by multiplying by  $2\pi$  and use symmetry to integrate the other side of the plate which doubles the total value. This simplified gradient model (with regards to unshared waves) considers both sides of the confinement to reflect the distribution and vector properties of the correlated vacuum fluctuations.

$$H_{tot} = 2 \cdot 2\pi H_{avg} = 8 \quad (15)$$

Finally use this integration factor to find the total theoretical force model which predicts the force amplitude that was observed.

$$\Delta F = \frac{8\hbar c N_e}{d^2} \frac{\ln(\frac{R}{d})}{\ln(\frac{2R}{l_p})} \quad (16)$$

## 4.2 Theoretical force model by Wave energy formula

One can also derive the theoretical model of the force by using the wave energy formula.

$$E = \frac{hc}{\lambda} \quad (17)$$

Now let us find the total wave energy in the confinement region letting  $\lambda = 2kl_p$  to count all the waves up to  $N$ . Here the  $l_p$  comes from the fundamental wavelength.

$$\sum_{k=1}^N \Delta E_d = \frac{hc}{2l_p} + \frac{hc}{4l_p} + \dots + \frac{hc}{2Nl_p} \quad (18)$$

Plug in for  $\lambda = 2kl_p$  in order to count all the waves in the Rindler region up to  $M$ .

$$\sum_{k=1}^M \Delta E_R = \frac{hc}{2l_p} + \frac{hc}{4l_p} + \dots + \frac{hc}{2Ml_p} \quad (19)$$

Now compute the ratio of fractional energy that will be pushing the capacitor. Namely, the ratio  $\frac{\Delta E_R - \Delta E_d}{\Delta E_R}$ .

$$\frac{\Delta E_R - \Delta E_d}{\Delta E_R} = \left( \frac{\frac{hc}{2l_p} + \frac{hc}{4l_p} + \dots + \frac{hc}{2Ml_p}}{\frac{hc}{2l_p} + \frac{hc}{4l_p} + \dots + \frac{hc}{2Ml_p}} \right) - \left( \frac{\frac{hc}{2l_p} + \frac{hc}{4l_p} + \dots + \frac{hc}{2Nl_p}}{\frac{hc}{2l_p} + \frac{hc}{4l_p} + \dots + \frac{hc}{2Ml_p}} \right) \quad (20)$$

Now write the equation in closed form and simplify. Notice the common terms will factor out and cancel and will be the same result as (5).

$$\frac{\Delta E_R - \Delta E_d}{\Delta E_R} = \frac{\sum_{k=1}^M \frac{1}{k} - \sum_{k=1}^N \frac{1}{k}}{\sum_{k=1}^M \frac{1}{k}} \quad (21)$$

Follow the steps in previous derivation to finally result in the following where the force is over confinement region,  $d$ .

$$\Delta F = \frac{hcN_e}{d^2} \frac{\ln(\frac{R}{d})}{\ln(\frac{2R}{l_p})} \quad (22)$$

Following the same procedure in the uncertainty derivation and multiplying (22) to (14) and doubling it for both sides of the plate, the force formula will be the same as (16).

$$\Delta F = \frac{8hcN_e}{d^2} \frac{\ln(\frac{R}{d})}{\ln(\frac{2R}{l_p})} \quad (23)$$

In general, the overall force will be established by multiplying the force of a single acceleration event with the number of particles (electrons) involved over the duration of one second as determined by the electric current flow which is the total burst amount of accelerated particles. For the stacked capacitor, the overall force corresponds to the multiplication of the number of particles times the number of acceleration stages. Essentially, this is the force times the overall number of accelerated events within one second.

## 5 Discussion

While conducting a variety of capacitive discharge experiments from 2017-2019, a directional force was repeatedly observed in parallel capacitive charged plates during field emission and insulation breakdown discharge.

The experimental data highlighted:

1. A linear correlation between the thrust force and the accelerated mass.

2. With a decrease of the capacitor electrode distance, an exponential increase in the observed force was found while keeping the accelerated mass constant.

The effect was only observable and repeatable under certain conditions:

1. With a very short capacitor plate separation distance.
2. Under a uniform discharge with only electrons being the charged accelerated particles.

It appears that if an electric discharge occurs, such as bridging the electrodes by arcing, this would introduce positive charges to the system which would hinder the effect. Additionally, the force appears reversible when conductive material, insulated from the cathode, is inserted right behind the cathode of the capacitor. Furthermore, placement of the conductive material past the rindler horizon,  $R$ , also changes certain behaviors of directional force depending on if the material is connected to the cathode or not. Finally, extending the cathode thickness, between  $R$  and the cathode, can also decrease the normal effect. Similar testing was performed adding conductive material in front of the anode. The results were equal to the normal effect.

A simulated physical model was refined predicting measured force values by using aspects of the uncertainty principle and concepts derived from the theory of quantised inertia. Vacuum fluctuation of a confined quantum field was done using a simple equation using virtual particles (photons, Unruh radiation). This was derived from the information boundary of a Rindler horizon and the information deflection scenario of the anode inside the electron propagation path. This created an energy gradient. In general, this would have to be sufficiently high to become observable.

The present results, due to the clear operational characteristics of the trend lines and 507 data points collected for charts, allow for the positive identification of a new effect. The prototype thruster concepts can be modeled with an equation based on some concepts as outlined by theory of quantised inertia [7] [8] and using discrete Unruh waves with nodes at the horizon. Since the predictive model and the experimental results are very closely converging, and no other models exist explaining the effect without violating the present law of physics, the result may also denote that an Unruh-like radiation physically exists. This could be by quantum field oscillations and symmetry breaking which enables forces which were observed in this experiment.

From all four sub-experiments, it is proposed that confined quantum field oscillation is composed of a discrete spectrum. This particular confinement scenario and causal information confinement by a Rindler horizon can be used for practical applications. The experiment has shown that a Rindler horizon physically exists. Additionally, an associated horizon radiation may cause an alteration in the energy state distribution of virtual particles and, in turn, provides a means to modify accelerative conditions. Furthermore, as the identified thrust force acts in the general inertial framework, this experiment may provide the basis of certain aspects of the theory of quantised inertia.

With regards to the topic of vacuum fluctuations of virtual particles in the confinement by the anode, it could be speculated that this is caused by the end of the field lines on an electrical horizon. For example, the accelerated electrons have their own

wavelength for which the thickness of the anode material would disallow the penetration. Therefore this limits the possible interaction of the electrons and their forward path world line and they would experience full attenuation as seen in particle/wave duality. Furthermore, Unruh radiation photons, which are experienced by the electrons, would not be able to penetrate through the anode plate thickness so the vacuum fluctuations, which are able to propagate in the seeing zone, would be virtual particles created at the location of the anode. This also suggests that the anode may operate as an equivalent causal event horizon. These experimental results suggest further research on this mechanism is recommended, namely, inspecting the physical feature of the anode which could act as an information horizon which appears to be observable. Additionally, artifacts are considered to be of a low probability due to the merging trend lines with different experimental setups. This would exclude the fact that two different artifact disturbances could provide data points on the same curve for the device.

In another view, one could consider the inside zone between the cathode and anode to be correlated to the conventional Casimir effect. An electron immersed in this quantum state environment, having an acceleration and by that a Rindler horizon, would be under the influence of an additional field which corresponds to the radiation emitted by the Rindler horizon. Hence, the electron might be under the influence of two overlapping fields of quantum states. This would provide an energy/momentum gradient in the fields which, by conservation of momentum law, would initiate a resulting force effect due to the natural symmetry breaking. This would alter the normal natural radiation which causes inertia. The electron would float inside a casimir scenario in between the electrodes. Here, the radiation difference around the electron is not homogenous compared to the normal Casimir effect. Rather, the addition of the Rindler horizon radiation causes it to become inhomogeneous.

The new battery-powered onboard wireless setup resulted in successful bi-directional thrust. A thrust of approximately 10 mg was commonplace for the 20um capacitor with shunt currents matching the wired setup. Earth's magnetic field was around 45uT (measured) and an overestimate max length of 0.5 m for supply wires with a draw current of 0.5A in the primary circuit (measured and specs) was used. Additionally, the wires ran vertically and twisted so would unlikely result in any appreciable Lorentz forces. Even in a theoretical maximum scenario, the influence would be in the 1 mg range and would not affect the overall plausibility of the results. Additionally, a large magnet was placed in the vicinity of the DC wires and there was no noticeable effect during operations. It seems magnetic fields do not have an appreciable impact. This was expected using vertically twisted wires. Furthermore, the capacitor device direction was flipped without any change to DC circuit wiring, therefore, any Lorentz forces would be always in one direction. Finally, when the blocker was connected to the anode, no ionic wind effects were noticed when two positive plates surrounded the cathode.

With regards to a prototype thruster (quantum vacuum thruster), evidence collected would support the claim that the construction of a modular capacitor system, scalable and with relatively low power consumption, could indeed be feasible. The prototypes in this paper have a performance above 0.4 N/kW. This is a performance that Dr. H. White (NASA's SSRMS Subsystem Manager) considers a minimum requirement for a crewed mission to Titan/Enceladus [14]. Construction of modular stacked segments

could also provide an advantage by using individual segment shut-downs in case of failure/malfunction without compromising the thrust performance of the remaining part of the capacitors. Since the thruster concept is exclusively electric, this experimental discovery could provide a first tangible means for interstellar space exploration once an adequate source of energy is fine-tuned (see performance chart Fig. 9.)

## 6 Conclusion

By conducting tests on capacitive systems which accelerate electrons at values on the order of magnitude of  $10^{19}$  [ $\text{m s}^{-2}$ ] during field emission, a force accelerating the overall system has been clearly identified and characterized. This thrust force, observed distinctively in capacitors with a minimized distance between the electrodes, has a linear correlation with the amount of accelerated matter. This matter directly corresponds to the electrons released through an electric current determined by field emission. The force occurs when the causal propagation zone is confined to less than 50% of the acceleration associated with the Rindler horizon distance. The force is directed in the propagation direction, but can be reversed by attenuating the associated horizon boundary (Unruh) radiations within the Rindler zone. This can be done by placing conductive material at specific distances in the area behind the cathode, thus outside the capacitor. In these instances, the attenuator is electrically insulated from the cathode. Additionally, extending the cathode decreases the normal force proportionally by distance and can also create a force reversal if extended past the Rindler horizon.

Throughout the experimental tests it was identified that the force increases exponentially when distance between electrodes is decreased. Additionally, the force detection was confirmed in a soft vacuum and had a lower standard deviation compared to the non-vacuum collected data. Furthermore, the observed phenomenon does not seem correlated to any evidence collected while testing ion lifters [10]. In fact, the “thrust anomaly” is assumed to be caused by electrons accelerated within a capacitor due to a field emission from a high electric field. To observe this thrust, it is paramount to keep the distance between the electrodes at minimum. No observable effect was seen when a control capacitor was placed with significantly thicker insulation between the plates into the measurement apparatus.

The observed thrust can be enhanced by preheating the capacitor so that the energy value required by the electric field for electron transmission can be lowered by means of Schottky/thermionic effects. In addition, the field strength can be increased by changing the field type from homogeneous to inhomogeneous. For instance using sandpaper or applying a high number of small cuts on the cathode surface can facilitate field emission. Furthermore, the force can be multiplied by using a modular design of stacking capacitors in series. This architecture, with respect to a single higher performing capacitor, has the advantage of keeping each segment performance independent from the remaining ones.

The indirect discovery of the existence of Unruh radiation and/or coupled with vacuum fluctuations which align in discrete waveforms between information horizon (or some other oscillatory nodal waves with information boundaries within the zero point field of virtual particles, suggested abbreviation as QVO “quantum vacuum oscillations”) demonstrates a net force in accordance to a physical model aligned with core

concepts initially outlined by McCulloch's theory of quantised inertia. The experiment has shown that a Rindler horizon physically exists and this horizon radiation provides a means to modify accelerated conditions.

The capacitors tested in the experiments have a performance above 0.4 [N/kW]; a benchmark often used by NASA to define a thrust ratio sufficient for interplanetary travel. In fact, this simple technology has the advantage of being completely electric; thus, suitable for fuel-less electric propulsion in vacuum. Coupled with adequate energy source generation, the scalability of this architecture might be appropriate for interstellar travel and precise maneuvering in space.

Looking into the experimental trend results, it seems essential to conduct the experiment with more accurately calibrated measuring equipment. It is also suggested that next scientific efforts should focus on correlating these results with an existing theoretical framework so this apparent anomaly can be adequately predicted and controlled for practical engineering purposes. Thus far, the preliminary correlation results are certainly encouraging. A second priority would be to test and/or prepare this apparatus in space to validate its performance in a vacuum to note its performance away from a strong gravity source.

## 7 Acknowledgments

We would like to express gratitude to the persons who assisted in experimental development as well as the facilitation for the results and compilation of this document. In particular we would like to thank Prof. Dr. M.E. McCulloch for encouraging us and providing us directions. For assisting in our early experimental stage setup, we would like to say thank you to Tommy Callaway. Furthermore, we appreciate the open minded discussions with John Doorman and Fabio Zagami on many general related subjects. Finally, this research would have never taken place if F.W. Becker would have not, decades ago, supported one of the authors (his son) and provided him the first means to see the initial observation of the effect in a science laboratory. The authors would like to express gratitude to both their families for supporting their academic endeavors.

## 8 Appendix A: Alternate Theoretical Model

Here, inspect the seeing zone conditions where the more precise seeing zone length is (with  $\beta = 0.2014$  pers. comm. McCulloch) and  $4\beta\pi^2 = 7.951$ . For simplification consider the maximum wavelength as suggested by McCulloch to be approximately 8 Rindler distances. Basically 7 more oscillations compared to the fundamental wavelength of the Rindler zone are allowed inside the propagation path. Using (1) this results in the approximated unshared wave energy level simplified to:

$$\sum_{k=1}^{8-1} \frac{k}{8R} hc \tag{24}$$

Here,  $R$  is the Rindler distance. From the sum computation, this yields an approximate constant factor of  $6.925 * 10^{-25}$  [J m] which can be multiplied by  $1/R$  to determine

the delta energy of the un-attenuated accelerated inertial condition (by considering the contribution of the unshared waves). Let us call this parameter, since it is relevant for a 1 meter definition for the time being, the inertial energy factor due to the dimensional unit of [J m].

The quantised seeing zone energy of the unshared oscillations would require the equilibrium to cross the abscissa  $x$ -axis at one Rindler distance. Furthermore, in the un-attenuated confined state, the energy level at  $8R$  should be the same as computed by the inertial energy factor for the inertial undamped state. In this case, the number of allowed unshared waves is 7 which is used for the total summation function.

For curve fitting, the following equation can be created to match the seeing zone equation for a more general  $x = R$  situation to find the constant 7.111 by adjusting the output value to the same value as the ‘inertial energy’ factor for 1 meter. Basically, this is accomplished by setting the confinement length to  $d = 8$  Rindler lengths.

$$\Delta E = \sum_{k=1}^7 \left( \frac{8-k}{8^2} \right) \frac{7.111k}{8} hc = 6.925 * 10^{-25} \quad (25)$$

The numerical determination of the seeing zone energy factor will be 7.111/8. Below the number of unshared waves can be computed by an integer variable that is dependent on the ratio  $d/R$ .

$$\Delta N = \lceil 7.5 - \left( \frac{7}{1} - \frac{d}{R} \right) \rceil \quad (26)$$

Now one can replace the value 8 in (23) with a more general confinement position  $d$  to find energy behavior over the change in the confinement distance while still keeping the previous numerical estimated seeing zone related energy factor of 1/1.125.

$$\Delta E = \sum_{k=1}^{\Delta N} \left( \frac{d-R}{d^2} \right) \left( \frac{7.111k}{8R} \right) hc \quad (27)$$

The overall situation can be represented by the following.

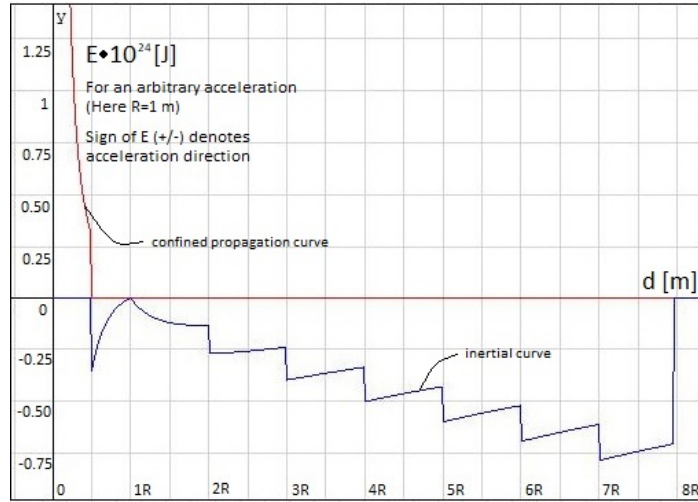


Figure 26: Approximation of energy delta profile in confined seeing zone

By the engineering approach of curve fitting between the 2 extrema of the zero cross equilibrium at  $1R$  and the un-attenuated original inertia situation energy level at approximately  $8R$ , it appears that the identified fitting parameter of  $7.111/8$  would refer to the factor  $1/1.125$  which corresponds to the increase in the original wave energy of the individual steps up to the point where the one wavelength is cancelled out by reduction of confinement distance. Notice the overall curve is valid for a confinement  $d > 0.5R$ .

In Fig. 26 at a given Rindler length inside the propagation path, a confinement situation is established which reduces the quantised wavelength in front of an accelerated particle.

An interesting note is that between  $0.5R$  and  $1R$  the absolute energy delta increases with a further confinement length reduction. This correlates to the situation where the energy in the Rindler zone is constant and the same wave number in the propagation path exists, but due to shorter confinements, a slightly shorter wavelength (as limited by the maximum allowed fundamental wavelength and the compulsory nodes at the boundaries) provides a higher energy level in the confinement zone. This continues until a confinement position of  $0.5$  Rindler length, where the fundamental wavelength is cancelled.

Fig. 26 does not include the consideration that all wavelengths in the confinement are shorter compared to all allowed wavelengths in the Rindler zone (as this only focuses on the unshared wavelength contribution to the energy delta). Hence, this is simply a first illustration of the energy profile in a case where the seeing zone confinement is applied.

## 9 Appendix B: Skin Depth

Below is the simplified skin depth equation for good conductors.

$$\delta = \sqrt{\frac{2\rho}{2\pi f \mu_r \mu_0}} \quad (28)$$

$\rho$  = resistivity of the conductor

$f$  = frequency of current

$\mu_r$  = relative magnetic permeability of the conductor

$\mu_0$  = the permeability of free space

## 10 Appendix C: Potential Errors

The results during both the remote (battery powered unit without exposed HV conductors) and wire testing could result in “Trichel pulses” by insufficient insulation. The signature of these pulses have the properties of lifted currents (offset = DC component with sharp inrush currents) as seen on the oscilloscope display. The signals look similar to field emission currents but have different attributes (spikes), and are actually a corona discharge with trichel pulses. Field emission events occur having current peaks starting from approximately zero on the display of the oscilloscope. In contrast, externally located trichel impulses (in wiring etc.), which are generated outside the test capacitor, do fluctuate but are added in amplitude to the small DC component leakage current. It was found that a leakage current is likely generated from a conductive enclosure such as the Faraday shielding cage without sufficient inner insulation material near a thin high voltage charged conductor. Here, it would also be relevant to check the insulation rating when appropriate since, for example, a 500 V rating would be insufficient as a direct barrier between HV polarities. Usually, 500 V is typically a standard value rating of insulators on the market. Furthermore, an air layer with the insulation material of a conductor could become a composite capacitor (voltages distribute with each material index and per thickness involved). The electric field strength inside the air is significantly higher than inside the material. Therefore if a metallic object such as a shielding enclosure is connected to the negative polarity, electrons could be tunneled out the surface due to insufficient insulation and ionize the air gap to the next conductor. Additionally, using conductors not rated appropriately to the intended use could also lead to a null effect due to leakage currents. Additionally, having twisted conductor supplies inside sheeted routing should not be near an enclosure which could have a different polarity. If the field is strong enough, the electrons could be pulled out of the enclosure and accelerated towards the insulator.

One can also consider the influence of possible Lorentz forces even though the HV supply current is significantly low. One solution is the usage of twisted conductors. However, this should be done with care as twisted conductors with different polarities with longer lengths could also cause leakages. Hence it should be seen essential to provide twisting with limited/avoided direct contact of insulation of conductors with different polarities during a high voltage scenario. During twisting, application of air loops may boost insulation distance and limit the direct contact points. Also, it is necessary to utilize conductors rated for the high voltage application. Adding tubing over high voltage conductors rated up to 500V (working voltage, insulation voltage) should be considered an insufficient insulation system if there is direct contact with

one conductor (Faraday or conductive mu-metal surface connected to one HV polarity). Recreation of the Trichel pulses were performed in January 2019 during further testing. The result usually ended in a null effect since the path of least resistance was not through the capacitor. Larger currents around 10uA were commonplace to be measured at the shunt. These currents were far too high for a low power 10W supplies or below. If this is observed with no force effect, it is most likely related to tracking, leakage currents and trichel discharges. For a valid effect, values were nominally much lower in the low uA range for a large normal effect. Power supplies with internal current monitoring should not replace the essential monitoring of a real oscilloscope. This is necessary to identify the field emission of current. These are common complications/mistakes by an experimenter who lacks sufficient skill to achieve adequate experimental setup conditions. Furthermore, a voltage drop, such as supply voltage decreasing by half, across electrodes or at the output of the power supply is a signature for tracking complications. Experiments under these conditions should not be conducted before further investigation and troubleshooting.

At the current state of research it is not yet clarified whether the quantum vacuum oscillations emerge from the local vacuum or are emitted by the cosmic horizon [7]. A mu-metal shielding might cause complications during testing so in the future it is suggested to compare the use of normal Faraday cages and mu-metal cages.

## 11 Appendix D: Additional Testing

Additional verifications tests performed during 2020-2021 have included the following: application of light including UV to electrodes, Radioactive elements (radium) applied on electrodes, various methods of heating onboard to device including resistive pad heating, glow in the dark paint on electrodes, Fine sanded aluminum, liquid application to cathodes, Carbon nanotubes (CNTs) placed on electrodes with and without pulsing DC with modulation. Heat application to electrodes in conjunction with all of the above was performed as well.

It was concluded adding carbon nanotubes (rolled graphene) powder or film and applying it to the cathode would increase the level of field emission overall. [17] [18] This resulted in a larger amount of electric current (accelerated electrons) at the same voltage. The comparison was done on 20 micrometer capacitors with carbon nanotubes versus one without. Partial discharges and field emission current was typical to peak at over a 5x increase with same capacitor size in terms of surface area.

Also one can apply an increased surface area and this will allow less points of failure (such as device ruptures) due to current density being spread out during the sweeping of voltage up to 5kV. Overall this will lead to a higher thrust value. The carbon nanotubes seem to provide an individual capacitance property due to a galvanic discontinuation of conductivity by contact resistance of the cathode plate to the nanotubes. It can be assumed that such device has more simultaneous discharges by increasing the surface size. Using carbon nanotube (CNT) in conjunction with a pulsing DC waveform could be used to create field emission effect and help maintain a higher overall field emission over time. It has been concluded that a DC pulsing waveform (sawtooth, sine, etc) will alter the  $dV/dt$  properties of the capacitor supply waveform and should facilitate to jostle and liberate an increased level of electrons off from the cathode.

Using this in combination of Carbon nanotubes (or other materials with many sharp points to increase field strength, such as geometric means of cathode array technology on cathode or other cathode surface enhancements) could get a higher and more stable field emission current. However, partial discharges are seen readily with most plastics (organic) insulators due to the presence of material voids so this must be taken into caution.

Different sized capacitors were used and field current increased with area when using the CNTs. In general it would be prudent to try many different types of available pulsing waveforms in combination with cathode surface conditions having various the geometric shapes. An optimized waveform might vary for each type of dielectric such as glass, ceramics, plastics polyamide, silicon dioxide etc.

Most insulating plastics used as dielectric plate separator had partial discharges during sweeping of voltage. This became even more apparent as the thickness of the insulator sheets were reduced. Thicknesses of 2 micrometers to 20 micrometers were tested. Even though a larger force could be attained during this condition, the dielectric quickly degraded and would lead to failure (reduced lifetime). Therefore, for a performance test, one might obtain high thrust values temporarily, but it is not practical from a reliability standpoint since the force would be proportional to the number of voids and area of the surface, but the reliability as a commercial product into the industry would be affected.

In addition many liquids were applied to the cathode during testing. These included vinegar with ammonia, various waxes, distilled water to name a few. Some did boost the field emission and could be beneficial.

Further testing for advanced applications could be very promising in the future. Using Aluminum nano-particles on electrodes, Polymer films with embedded metal nanoparticles, Nano-etched electrodes are potential ways to increase the field strength and performance including a condition to achieve a higher amount of simultaneous accelerated charge propagation.

## 12 Appendix E: Time Graphs

Below is an example summary of testing of the wired setup for 20 micrometer capacitors using the flyback. This was done to show a constant thrust value over time. Quick impulses of current may give high thrust values for a short time frame but to obtain a practical device a steady state thrust signature is ideal and is shown to be capable here.

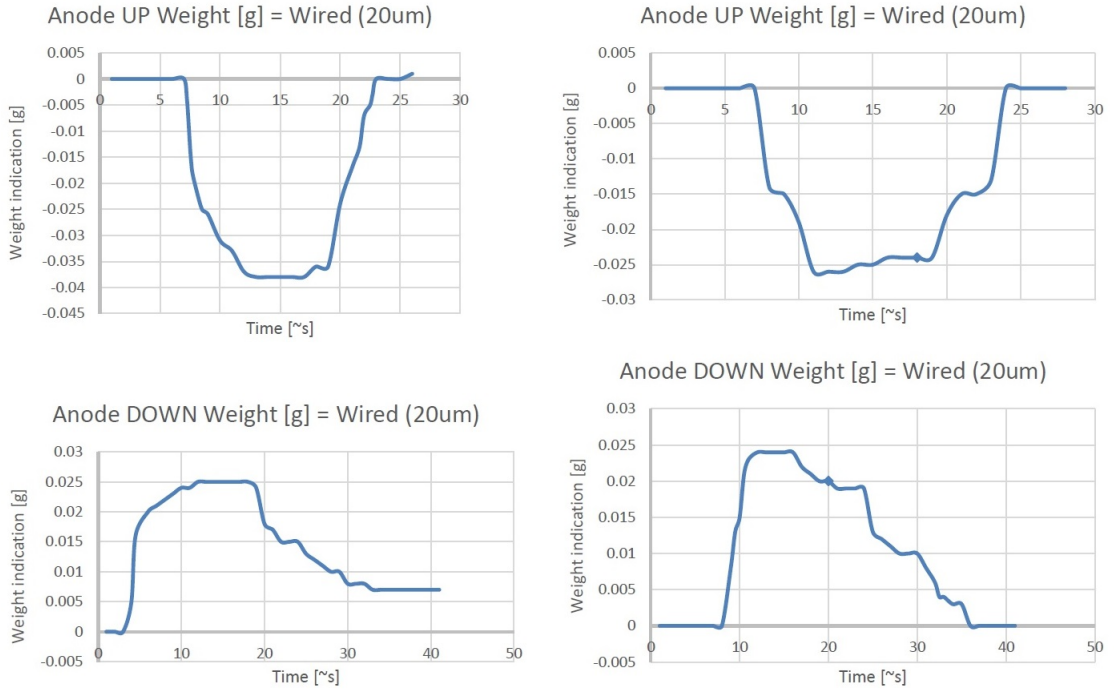


Figure 27: Time Graphs for Wired Setup 2021

## References

- [1] A. Froebel. Cable shielding to minimize electromagnetic interference. *EEEIC*.
- [2] D. Go and D. A. Pohlman. A mathematical model of the modified paschen's curve for breakdown in microscale gaps. 107:103303 – 103303, 06 2010.
- [3] S. Harjo. Partial discharge in high voltage insulating materials. 8:147–163, 03 2016.
- [4] S. W. Hawking. Evaporation of two-dimensional black holes. *Phys. Rev. Lett.*, 69:406–409, Jul 1992.
- [5] Y. Lau and Y. Liu. From fowler-nordheim relation to the child-langmuir law. 1994.
- [6] M. Mcculloch. Inertia from an asymmetric casimir effect. 101, 02 2013.

- [7] M. McCulloch. Low-acceleration dwarf galaxies as tests of quantised inertia. 362, 03 2017.
- [8] M. E. McCulloch. Minimum accelerations from quantised inertia. *EPL (Europhysics Letters)*, 90(2):29001, 2010.
- [9] E. L. Murphy and R. H. Good. Thermionic emission, field emission, and the transition region. *Phys. Rev.*, 102:1464–1473, Jun 1956.
- [10] M. Tajmar. Biefeld-brown effect: Misinterpretation of corona wind phenomena. *AIAA Journal*, 42(2):315–318, Feb 2004.
- [11] R. L. Talley. Twenty First Century Propulsion Concept. Technical Report F04611-89-C-0023, VERITAY TECHNOLOGY INC, May 1991.
- [12] W. Unruh. Acceleration radiation for orbiting electrons. 307:163–171, 04 1998.
- [13] W. G. Unruh. Notes on black-hole evaporation. *Phys. Rev. D*, 14:870–892, Aug 1976.
- [14] H. G. White. Q thrusters. In *Pilot Wave Model for Impulsive Thrust from RF Test Device*, Breakthrough Discuss - Day Two, 2018.
- [15] E. M. Vogel, K. Z. Ahmed, B. Hornung, W. K. Henson, P. K. McLarty, G. Lucovsky, J. R. Hauser, and J. J. Wortman. Modeled tunnel currents for high dielectric constant dielectrics. *IEEE Transactions on Electron Devices*, 45(6):1350–1355, June 1998.
- [16] K. Kokurewicz, E. Brunetti, G. H. Welsh, S. M. Wiggins, M. Boyd, A. Sorensen, A. J. Chalmers, G. Schettino, A. Subiel, C. DesRosiers, and D. A. Jaroszynski. Focused very high-energy electron beams as a novel radiotherapy modality for producing high-dose volumetric elements. *Scientific Reports*, 9(1):10837, 2019.
- [17] W. I. Milne, K. B. K. Teo, G. A. J. Amaratunga, P. Legagneux, L. Gangloff, J.-P. Schnell, V. Semet, V. Thien Binh, and O. Groening. Carbon nanotubes as field emission sources. *J. Mater. Chem.*, 14:933–943, 2004.
- [18] T. Kariyawasam. Field emission of carbon nanotubes. [http://www.phys.lsu.edu/~jarrell/COURSES/ELECTRODYNAMICS/Student\\_Projects/tharanga/review.pdf](http://www.phys.lsu.edu/~jarrell/COURSES/ELECTRODYNAMICS/Student_Projects/tharanga/review.pdf)
- [19] O. Tsui Capacitors with Dielectrics [http://physics.bu.edu/~okctsui/PY106\\_lecture\\_notes/class08.pdf](http://physics.bu.edu/~okctsui/PY106_lecture_notes/class08.pdf)